2024 IEEE International Conference on Robotics and Automation (ICRA 2024)
May 13-17, 2024. Yokohama, Japan

A scalable monolithic 3D printable variable stiffness mechanism

Paul Baisamy[1], Adam A.Stokes[1], Francesco Giorgio-Serchi[1]

***Abstract*— Variable Stiffness Mechanisms (VSM) are becoming ubiquitous in mechatronics given the benefit they provide in terms of safety and performance. Despite these assets, VSMs remain fairly complex mechanical devices lacking in compactness, ease of manufacturing and accessibility. In addition, the scarcity of commercially available VSMs requires that such systems are mostly designed in-house. We propose a new type of VSM that improves on the pre-existing Jack Spring concept by making it more compact and robust. The new concept, which we refer to as the Compact Modifier of Active Coils (C-MAC) mechanism, is specifically designed to be manufactured through a monolithic 3D print. This approach enables to modify a minimal set of design features, namely the spring diameter and the coil diameter, to achieve the desired range of stiffness variation. We test the proposed design on six configurations; these show hysteretic energy losses no larger than 35% over the stiffness variation and confirm stiffness to scale according to theory. Stiffness ranging from 0.15 N/mm to 1.02N /mm were measured for an overall device length of 140 mm, including a maximal stroke length of 22 mm. The results confirm excellent scalability and manufacturability of the proposed design, providing a versatile mechanism for fast prototyping and the development of entire 3D printed robotic systems embedding variable stiffness capabilities.**

I. INTRODUCTION

Variable stiffness mechanisms (VSMs) have gained considerable traction in robotics due to the remarkable benefits they bring in terms of safety and dynamic performance. Adjustable impedance represents an essential feature of VSMs which makes human-robot interaction intrinsically safer, facilitating the adoption and acceptance of robots across applications ranging from entertainment to industrial assembly lines. In addition, fine control over joint stiffness represents a key asset in the development of advanced prosthetic devices as it contributes to generating motion more akin to the deficient limb. Importantly, VSMs have gained attention thanks to their ability to endow mechatronics devices with drastic locomotion efficiency gains via the exploitation of passive elastic energy storage [1]. Specifically, because energy expenditure is minimized when the locomotion gait is performed at the system's natural frequency [2], as the latter is directly dependent on stiffness [3], VSMs are essential to consistently match the robot's natural frequency to it's actuation frequency.

[1]P. Baisamy, A. Stokes and F. Giorgio-Serchi are with the Institute of Integrated Micro and Nano Systems, School of Engineering, University of Edinburgh, Edinburgh EH9 3FF, UK p.baisamy@sms.ed.ac.uk, a.a.stokes@ed.ac.uk, f.giorgio-serchi@ed.ac.uk. The authors gratefully acknowledge the support of the EPSRC CDT-RAS.

Stiffness tuning can be achieved with a wide range of approaches and the interested reader is referred to [4] for a comprehensive review of existing mechanisms. However, the vast majority of VSM commonly employed either use large and complex mechanisms [5], [6], [7], require high currents/voltages [8], [9] or constant input of energy [10] which may be suitable for specific applications but limit their use on a larger scale. Moreover, the scarcity of commercially available VSMs which can satisfy a broader range of design specifications and application scenarios often prevents their implementation in mechatronics systems where their employment would be beneficial. Indeed, it could be argued that in order to facilitate their adoption on a broader scale, VSMs would need to satisfy the following requirements: they should not operate on a constant energy supply to maintain a new level of stiffness, especially when used for energy gains, secondly, they should be compact and of limited design complexity to facilitate their implementation in pre-existing systems, thirdly, they should exhibit broad stiffness scalability in order to accommodate a large spectrum of design specifications and, ultimately, their manufacturing process should be optimized to reduce costs of production and lead time.

To address the above operational requirements, we propose a novel variable stiffness mechanism based on the modified Jack spring design of [11]. As its counterpart, our solution can be used as an adjustable robotic tendon in gait assistance devices as well as in any system submitted to linear motions such as jumping robots and vehicle suspensions or systems driven by voice coil actuators and solenoids. However, the present design drastically improves on the existing Jack spring approach of [11] by making it extremely compact and highly customizable from a stiffness range perspective. Most importantly, the proposed mechanism is specifically designed for monolithic manufacturing via 3D printing, thus ensuring inexpensive and speedy production. Moreover, as the development of fully 3D printed robotics solutions continues to gain considerable traction [12] [13], our design highlights the possibility of embedding variable stiffness in these systems paving the way for high performance cost effective solutions ready for mass manufacturing and quick on field deployment. In order to facilitate testing and uptake of the proposed design, this manuscript is appended with the parametric 3D files (a link to the repository can be found at [14]) aiming to provide the reader with a prompt and customizable solution for fast prototyping.

The first section of this manuscript introduces the design features of the proposed mechanism as well as the experimental setup used to evaluate its performances. It is followed

979-8-3503-8457-4/24/$31.00 ©2024 IEEE

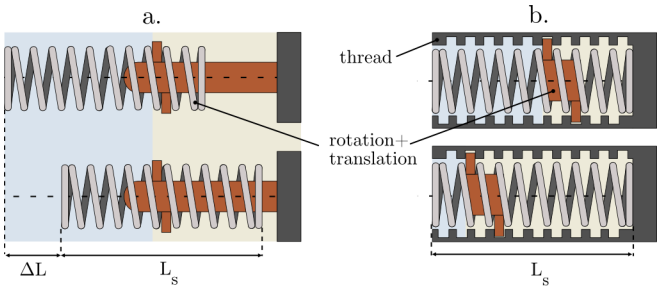

Fig. 1. (a) Original Jack Spring design concept. Rotation of the spring around the nut drives the spring translation along the nut axis, resulting in a change of the spring length on either side of the nut. When the number of coils is changed, the stiffness in the blue and yellow sections is modified according to eq. 1. The total length necessary to fit this system is $\Delta L + L_s$. (b) Proposed concept. The nut rotates and translates while the spring is static. The thread is used to make sure the nut does not translate when a load is applied on the spring. The total length necessary to fit this system is now only L_s.

by the analysis of the experimental results detailing the stiffening capabilities and efficiency potential of the device.

II. MATERIAL AND METHODS

A. Jack spring concept

The proposed VSM improves on the concept of Jack spring. A Jack spring has the same working principle of a leadscrew, with the exception of the threaded shaft being replaced by a spring. In other words, a leadscrew can be regarded as a type of Jack spring with an infinitely large stiffness. A schematic of the Jack spring mechanism is depicted in Fig. 1(a), where the brown-coloured component acts as a static nut around which the spring is allowed to rotate and translate axially. When the spring rotates, its length or, equivalently, the number of coils varies affecting the stiffness of each spring on each sides of the nut (blue and yellow shaded sections of the schematics in Fig. 1(a)). Indeed a spring's stiffness is inversely proportional to the number of active coils [15]:

$$k = \frac{d^4 G}{8 D^3 N} \tag{1}$$

where k is the spring stiffness, d is the wire diameter, G is the shear modulus, D is the mean coil diameter, $N = L/p$ is the number of active coils, with p the coil pitch and L the active length of the spring.

B. Compact Modifier of Active Coils (C-MAC)

We introduce a variant of the Jack Spring concept where the change in spring length is dictated by the combined translation and rotation of the nut, Fig1(b), as opposed to the translation and rotation of the spring itself, Fig1(a), as proposed in [11]. This modification, combined with specific design choices, allows for significant simplification in manufacturing terms as well as in compactness of the overall assembly.

The C-MAC VSM is detailed in Fig. 2. This is made of three constitutive parts: the *main body*, the *shaft* and the *slider*. The *main body* consists of the supporting structure, threaded on its lower section with a pitch p, of the spring

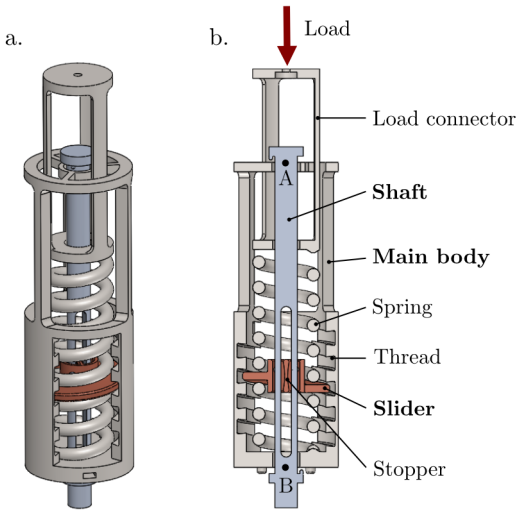

Fig. 2. (a) 3D view of the C-MAC Variable stiffness mechanism design. (b) Cut view with the key components annotated and the constraint points A and B of the *shaft*.

having the same pitch p and of the *load connector*. The *main body* is assumed to be completely static while the *load connector* acts directly on the spring and can translate axially to compress or extend the spring. The *shaft*, connected externally to an actuator which drives a rotation around its central axis, is constrained from translation by the *main body* at points A and B, Fig. 2(b). When the *shaft* rotates, the *slider* rigidly rotates along with it, thanks to the rotation of the *stopper*. Guided by the thread in the *main body*, the *slider* undergoes a rotation around and a translation along the *shaft* relative to the *main body* and, consequently, relative to the spring. This translation of the *slider* affects a change in the number of coils located in between the *load connector* and the *slider*, ultimately modifying the mechanism's stiffness. The spring section located in between the *slider* and point B is not affected by the load exerted by the *load connector*, because the *slider* and the thread prevent the force transmission to this part of the spring.

This C-MAC VSM offers a number of remarkable benefits over its predecessor. Firstly, the mechanism which modifies the spring's active coils is entirely contained within the spring itself, thus making the C-MAC much more compact than the Jack Spring. Indeed, as shown in Fig. 1, no additional length than the length of the spring itself L_s is required to fit this mechanism in a larger assembly, making the new design particularly compact. Consequently, for a given available length, the range of stiffness attainable is twice as high as the original design as no space has to be dedicated to spring translation. Secondly, this VSM lends itself to monolithic 3D printing by stereolithography, making it extremely simple, inexpensive and fast to manufacture.

C. Design for monolithic 3D printing

While the C-MAC can be manufactured with metals in traditional ways, it also lends itself to being entirely 3D printable. In addition to reduced lead time and cost of production, this feature allows individuals and institutions

without dedicated manufacturing capabilities (CNCs, lathes, milling machines) to easily produce custom VSMs, thus facilitating quick design iterations. Moreover, it emphasizes the possibility of designing entire high performance 3D printed robotics systems that can be mass manufactured for a fraction of their machined counterparts. The VSM design presented in this manuscript and in the supplementary material showcases a number of specifications intended for the purpose of monolithic 3D printing. These are reviewed here for readers' convenience and depicted in Fig. 3. In particular, purposely designed openings were added to either ensure the outflow of resin from the mechanism during printing or to prevent the creation of printing supports in places otherwise hard to reach. These features are essential to ensure a smooth functioning of the mechanism and an easy removal of the supports after printing. These are highlighted in Fig. 3(a) and (b) respectively, for the *slider* and the *main body*. These features directly affect the printing orientation and consequently the position of the printing supports. In particular, the openings and holes presented in Fig. 3(b) and (c) face the print bed. Similarly, the oblong cavity in the *shaft*, Fig. 3(a), is also facing the print bed. A 5°angle between the build plate and the axis running along the VSM shaft is added to reduce cupping effects between the part being printed and the resin tank in order to ensure that the part does not detach from the print bed. Finally, the slider was deemed best positioned around the centre of the openings in the main body threading so to reduce the likelihood of bonding with the main body.

Following an iterative design optimization process, we identified a number of minimal key dimensions which guarantee a robust product, Fig. 4. Firstly, all the clearances e in the system should not be smaller than 0.8 mm. Secondly, the spring wire diameter d should measure at least 2 mm. Thirdly, the thicknesses t_1 and t_2 (Fig. 4) should both be no lower than 1.5 mm and the stopper thickness no smaller than 1mm. Fourthly, the shaft diameter D_s should measure at least 6.5 mm. These are conservative values that should always ensure a good functioning but can be adjusted on a case by case basis. These key dimensions directly predetermine the values of the mean spring diameter D and the pitch p as follows:

$$D \geq D_s + 4e + 2t_2 + d \tag{2}$$

$$p \geq t_1 + d + 2e \tag{3}$$

The parametric 3D files used in this study can be found at [14].

D. VSM manufacturing

The VSMs were printed with a Formlabs 3+ (firmware rc-2.1.0-2005) with the Clear v4 resin (RS-F2-GPCL-04). The software used to generate the printing files was Preform 3.30.0. The VSM was positioned on the printing bed according to the recommendations given in section II-B. A layer thickness of 0.1 mm and a full raft with supports having a touchpoint size of 0.35 mm were used. The supports were

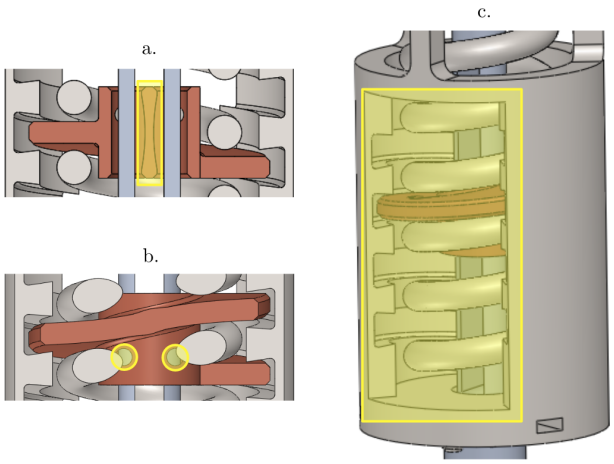

Fig. 3. Design features added to ensure proper 3D printing. Figure (a) and (b) illustrates features added to limit entrapment of the resin against the *shaft*. Specifically, the stopper is made concave and holes are added on the *slider* to facilitate the resin flow. The openings on Figure (c) are added in order to be able to access and remove the printing supports inside the *main body*.

generated by using the auto-generate function of the software with no internal supports. This ensures that, after removing the supports, few asperities remain on the thread, the *shaft* or the *slider* to guarantee a smooth functioning. However, when using the auto-generate function, a small amount of unsupported minima usually remain. Consequently, a few internal supports are added manually where needed.

After printing, the supports are removed and the parts are immersed in a bath of isopropyl alcohol (IPA) 99.9%. With a soft brush, excess resin is removed from the VSMs before putting them in a second bath of IPA 99.9% for ten minutes. The VSMs are given their final mechanical properties by curing them with 405 nm UV lights during eight hours. Finally, the supports are removed and silicone lubricant is applied to ensure a smooth functioning.

E. Experimental setup

In order to evaluate the performance of the proposed VSM, the mechanism is tested under compression and tension. Scalability of the mechanism is also addressed here by manufacturing six VSMs with different wire diameters d and mean spring diameters D. These six configurations are

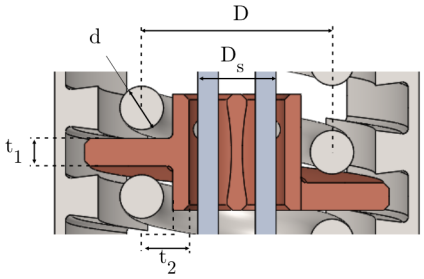

Fig. 4. Key dimensions for robust VSMs. D_s, d, t_1, and t_2 should be higher than 6.5 mm, 2 mm, 1.5 mm and 1.5 mm, respectively. These are conservative values that can be adjusted on a case by case basis.

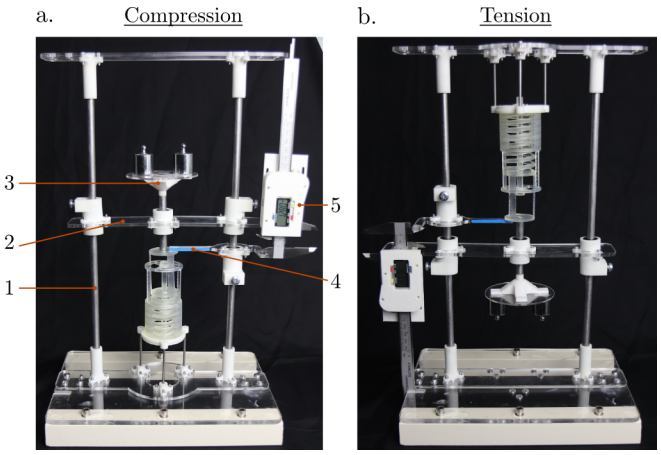

Fig. 5. Test rig used to perform stiffness measurements. It can be used both in compression (a) and traction (b).

Configurations	1	2	3	4	5	6
d (mm)	2	3	4	5	5	5
D (mm)	17.5	17.5	17.5	22.5	27.5	32.5

TABLE I

VSM CONFIGURATIONS FOR WHICH THE STIFFNESS WAS MEASURED.

presented in Table I. The overall length of each VSM is $140\ mm$ with a maximal stroke length of $22\ mm$.

Testing of the VSMs involved subjecting them to a prescribed force F which generates a displacement x. This displacement is measured to determine the stiffness as:

$$k = \frac{F}{x} \tag{4}$$

For each configuration, the stiffness was measured for 6, 5, 4 and 3 active coils.

The test rig presented in Fig. 5 was used to perform the stiffness measurements. This can be used for characterization of the compression, Fig. 5(a), and tension, Fig. 5(b), of the VSM. The test rig consists of the *main structure* 1, the *guiding platform* 2, the *weights holder* 3, the *measurement slider* 4 and the *caliper* 5, indicated in Fig. 5.

The procedure to perform a stiffness characterization in tension or in compression is as follows:

- Step 1: The VSM is installed on the VSM holder which is part of the *main structure* 1.
- Step 2: The *measurement slider* 4 is aligned with the top of the load connector and the *caliper* 5 is used to set the displacement at $x = 0\ mm$.
- Step 3: The weights are installed on the *weights holder* 3 which is connected to the load connector of the VSM. The weights holder translates in a straight line thanks to the *guiding platform* 2. A linear bearing is used to minimize friction.
- Step 4: After 30 seconds which ensure stabilization of the spring, the *measurement slider* 4 is realigned with the top of the load connector and the *caliper* 5 is used to measure the displacement x.
- Step 5: Steps 3 and 4 are repeated with new weights.

In each case, the VSM was first loaded and unloaded in compression and then loaded and unloaded in tension. In total, 28 repeated measurements were taken for each configuration.

Fig. 6. From left to right: VSMs in configurations 1 to 6 (Table I) after supports removal, IPA cleaning and additional curing in UV chamber.

III. RESULTS

The prints of the six configurations as per Table I are shown in Fig. 6. Following the protocol of section II-E, the data collected from the experimental test for each of these configurations is reported in Fig. 7, where the blue, orange, yellow and purple curves respectively correspond to 3, 4, 5 and 6 active coils. Fig. 7 brings evidence of a quasi-linear relationship between load and displacement of the springs associated with a slight hysteresis. The occurrence of non-linearities in the spring behaviour is mostly observed for smaller loads and especially for reduced number of active coils, Fig. 8(b). This type of non-linearity is not attributed to the spring material properties, but rather to the clearances implemented in the design to facilitate manufacturing. Indeed, as depicted in Fig. 8(a), systematic clearance of extent $c = p - t_1 - d$ arises when the VSM is at rest, due to the spring not engaging with the slider. In other words, when at rest, the VSM stiffness is not impacted by the slider's position and is always equal to the entire spring stiffness. However, upon loading the VSM the clearance c disappears and the relationship between stiffness and spring length is reinstated. This transition between two different stiffness profiles is responsible for the non-linearities observed. In particular, this phenomenon is prominent for low number of active coils because the stiffness increases when the number of coils is reduced.

Fig. 7 also highlights clear hysteresis loops for each case tested, underscoring the presence of internal viscoelastic losses. An estimate of the VSM's energy efficiency is obtained by integrating along the load curves, yielding the result in Fig. 9. The efficiency ranges between 0.64 and 0.88 across the whole range of coil activation and with an average of 0.78, confirming contained dissipation.

For what concerns derivation of the stiffness of the VSM, we rely on eq. 1. In order to determine the stiffness of the VSMs, a least squares linear regression is performed for each hysteresis loop of Fig. 7 and a shear modulus of $G = 401MPa$ provides the best fit for each of the

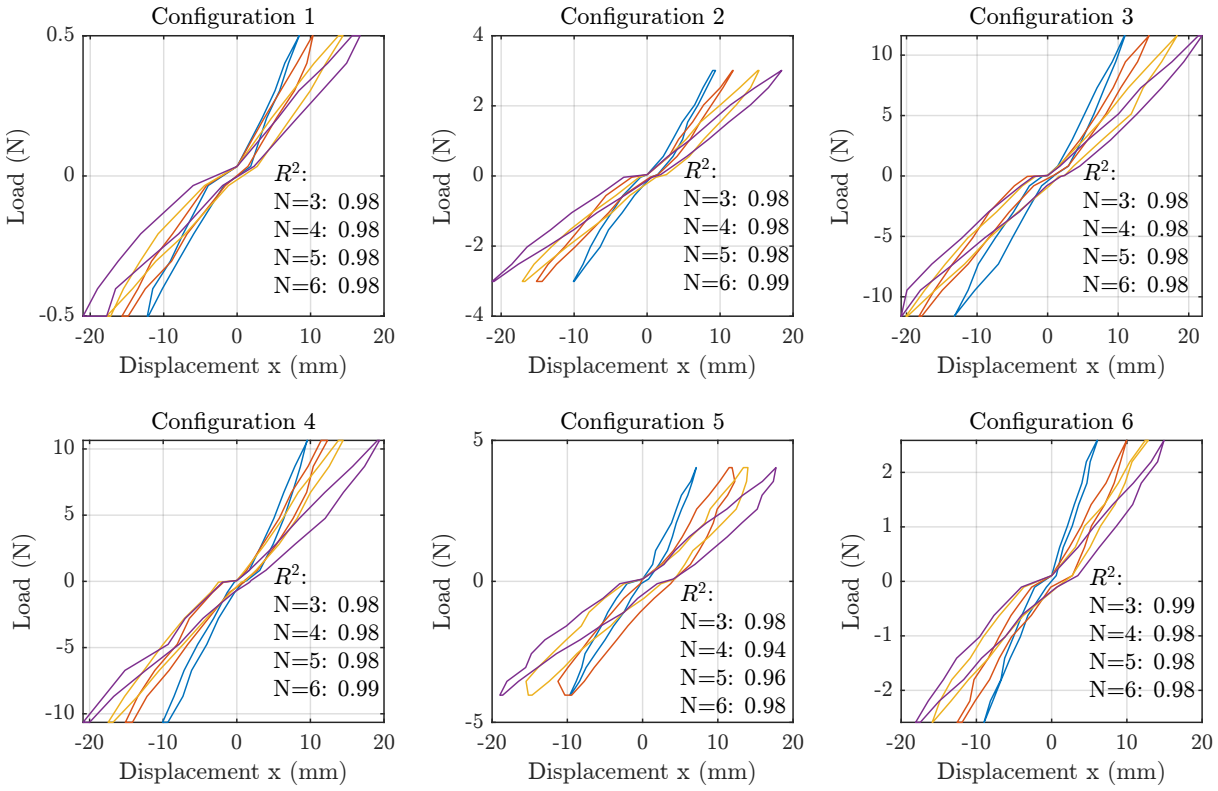

Fig. 7. Force versus deformation x for each configuration of VSM. Blue, orange, yellow and purple respectively represents 3, 4, 5 and 6 active coils N indicating linear stiffness scaling. The coefficient of determination R^2 in each subset indicates divergence from linearity for each case tested.

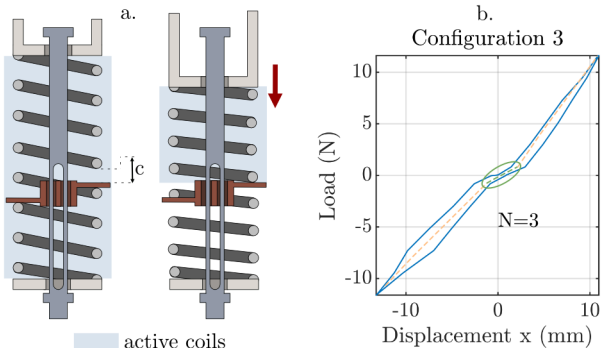

Fig. 8. Onset of non-linearity explained: a. Until the clearance c is present the VSM stiffness is dependent on the number of coils. However, once the load applied is sufficient to obtain $c = 0$, the stiffness is now dependent on the coils between the slider and the load connector. b. This phenomenon can mostly be observed for low number of active coils, as for instance, for configuration 3 with 3 active coils.

configurations tested. Using the shear modulus equation for isotropic material $G = E/(2(1+\nu))$[16], and assuming that the Poisson's ratio ν is in between 0.3 and 0.45 [17] while the Young's modulus E is in between 1.6 Gpa and 2.8 Gpa[18], the theoretical shear modulus is expected to range between 551 Mpa and 1077Mpa. While the value found with our experiments is lower than the theoretical minimal bound, the characteristics of the resin provided by the supplier data-sheet [18] emphasizes that its mechanical properties can be drastically impacted by temperature, part geometry and curing conditions, suggesting that values outside the nominal range are to be encountered. The coefficients of determination R^2 for each regression are presented alongside the curves in Fig.7. With $R^2 \geq 0.94$ the assumption of a linear stiffness profile is further confirmed. Values of R^2 are reported for all the reminder of stiffness measurements for readers' convenience.

Fig.10 and Fig.11, respectively present the stiffness as a function of spring mean diameter D and wire diameter d for different number of active coils. These are compared against the theoretical trends based on eq. 1. Finally, we assess the stiffness tuning performance of all the configurations

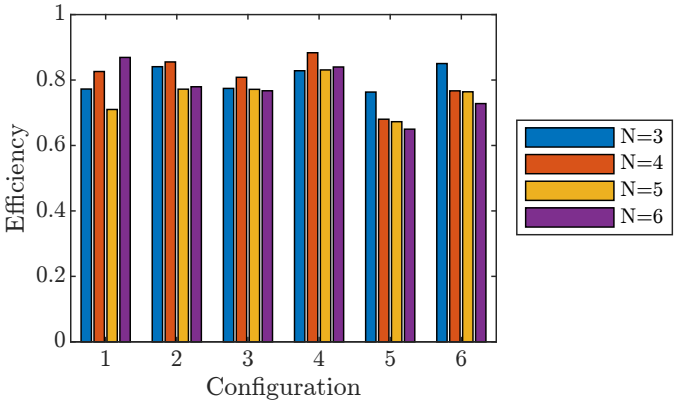

Fig. 9. Efficiency for each configuration of VSM and each number of active coils.

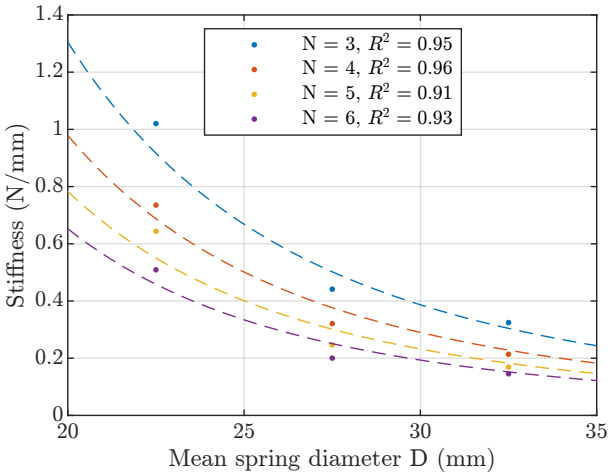

Fig. 10. Stiffness versus the mean spring diameter D. The dots represent the stiffness derived from the experimental data. The dotted lines represent the theoretical trends obtained with equation 1 with shear modulus G of $415.5MPa$.

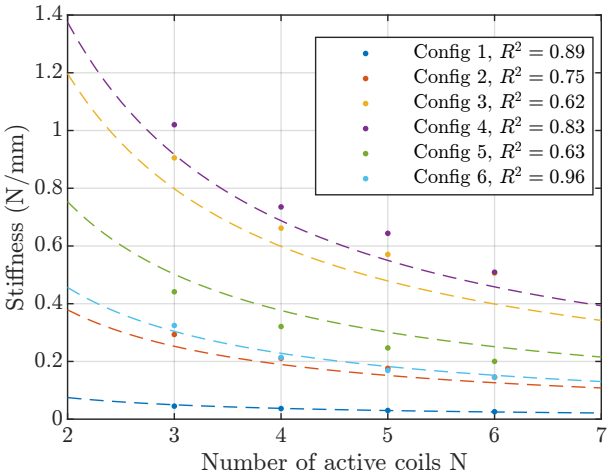

Fig. 12. Stiffness versus the number of active coils N for each configuration. The dots represent the stiffness derived from the experimental data. The dotted lines represent the theoretical trends obtained with equation 1 with shear modulus G of $415.5MPa$.

manufactured: Fig.12 depicts the stiffness variation as a function of number of active coils. The highest stiffness observed was 1.02 N/mm, obtained for configuration *four* with three active coils; the lowest stiffness of 0.15 N/mm was obtained for configuration *one* with six active coils. The range of $0.63 \leq R^2 \leq 0.96$ with a mean value $\overline{R^2} \approx 0.78$ gives confidence in the VSMs' performance closely matching theory and thus confirms that stiffness tuning scales with $k \propto N^{-1}$.

IV. CONCLUSIONS

We introduced the Compact Modifier of Active Coils (C-MAC), a concept of variable stiffness mechanism inspired by the Jack spring. Compared to existing stiffness tuning devices, its compactness, its low energy requirement to adjust the stiffness, its scalability and its ease of manufacturing makes it a highly sought after solution in robotics. In particular, we adjusted the design so that the assembled device can be entirely 3D printed by stereolithography through a monolithic print. Six variations with various wire and mean spring diameter were tested in compression and traction demonstrating that stiffness scales according to theory. A shear modulus value of $G = 401Mpa$ was found for the 3D printing resin used enabling to accurately characterize stiffness variation. The highest stiffness obtained was $1.02N/mm$ and the lowest $0.15N/mm$. Energy losses were observed with an average value of 22% confirming suitability of the proposed spring manufacturing for common prototyping purposes.

This 3D printing design has the potential to be used as a rapid and low-cost option and offers the chance to any enterprise in possession of an SLA printer to produce custom VSMs without having to rely on specialized manufacturing capabilities or on the very limited range of similar systems currently commercially available. It also highlights the possibility of developing and 3D printing entire high performance mechanical systems with embedded variable stiffness to facilitate the adoption of robotic systems through mass manufacturing and to accelerate their deployment on field. While the shear modulus of the resin used is significantly lower than the one of steel, resulting in lower spring stiffness for equivalent geometry, the C-MAC concept can promptly be fitted with metallic springs via minimal design retrofit for improved dynamic capabilities and durability. Finally, with metallic 3D printing becoming widespread, the C-MAC deign offers the unprecedented opportunity to manufacture high performance, highly customizable monolithic VSMs for industrial standard applications.

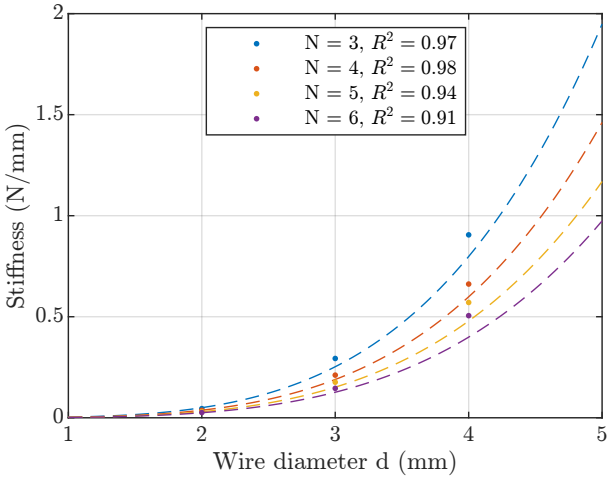

Fig. 11. Stiffness versus the mean spring diameter d. The dots represent the stiffness derived from the experimental data. The dotted lines represent the theoretical trends obtained with equation 1 with shear modulus G of $415.5MPa$.

REFERENCES

[1] S. Collins, A. Ruina, R. Tedrake, and M. Wisse, "Efficient bipedal robots based on passive-dynamic walkers," *Science (American Association for the Advancement of Science)*, vol. 307, no. 5712, pp. 1082–1085, 2005.

[2] T. Bujard, F. Giorgio-Serchi, and G. D. Weymouth, "A resonant squid-inspired robot unlocks biological propulsive efficiency," *Science Robotics*, vol. 6, no. 50, p. eabd2971, 2021.

[3] S. S. Rao, *Mechanical vibrations*. Pearson Education, 2017.
[4] S. Wolf, G. Grioli, O. Eiberger, W. Friedl, M. Grebenstein, H. Höppner, E. Burdet, D. G. Caldwell, R. Carloni, M. G. Catalano, D. Lefeber, S. Stramigioli, N. Tsagarakis, M. Van Damme, R. Van Ham, B. Vanderborght, L. C. Visser, A. Bicchi, and A. Albu-Schäffer, "Variable stiffness actuators: Review on design and components," *IEEE/ASME Transactions on Mechatronics*, vol. 21, no. 5, pp. 2418–2430, 2016.
[5] Z. Li, S. Bai, O. Madsen, W. Chen, and J. Zhang, "Design, modeling and testing of a compact variable stiffness mechanism for exoskeletons," *Mechanism and machine theory*, vol. 151, p. 103905, 2020.
[6] J. Sun, Z. Guo, D. Sun, S. He, and X. Xiao, "Design, modeling and control of a novel compact, energy-efficient, and rotational serial variable stiffness actuator (svsa-ii)," *Mechanism and Machine Theory*, vol. 130, pp. 123–136, 2018.
[7] M. Dežman and A. Gams, "Rotatable cam-based variable-ratio lever compliant actuator for wearable devices," *Mechanism and Machine Theory*, vol. 130, pp. 508–522, 2018.
[8] S. B. Behbahani and X. Tan, "Design and dynamic modeling of electrorheological fluid-based variable-stiffness fin for robotic fish," *Smart materials and structures*, vol. 26, no. 8, p. 085014, 2017.
[9] R. Carloni, V. I. Lapp, A. Cremonese, J. Belcari, and A. Zucchelli, "A variable stiffness joint with electrospun p(vdf-trfe-ctfe) variable stiffness springs," *IEEE robotics and automation letters*, vol. 3, no. 2, pp. 973–978, 2018.
[10] R. Van Ham, M. Van Damme, B. Verrelst, B. Vanderborght, and D. Lefeber, "Maccepa, the mechanically adjustable compliance and controllable equilibrium position actuator: A 3dof joint with two independent compliances," *International Applied Mechanics*, vol. 43, no. 4, pp. 467–474, 2007.
[11] K. W. Hollander, T. G. Sugar, and D. E. Herring, "Adjustable robotic tendon using a 'jack spring'," vol. 2005, pp. 113–118, 2005.
[12] T. J. K. Buchner, S. Rogler, S. Weirich, Y. Armati, B. G. Cangan, J. Ramos, S. T. Twiddy, D. M. Marini, A. Weber, D. Chen, G. Ellson, J. Jacob, W. Zengerle, D. Katalichenko, C. Keny, W. Matusik, and R. K. Katzschmann, "Vision-controlled jetting for composite systems and robots," *Nature (London)*, vol. 623, no. 7987, pp. 522–530, 2023. ObjectType-Article-1.
[13] P. Singh Matharu, Z. Wang, J. H. Costello, S. P. Colin, R. H. Baughman, and Y. T. Tadesse, "Sojel –a 3d printed jellyfish-like robot using soft materials for underwater applications," *Ocean engineering*, vol. 279, p. 114427, 2023.
[14] P. Baisamy, "A scalable monolithic 3d printable variable stiffness mechanism." Available at: https://github.com/pbaisamy/A-scalable-monolithic-3D-printable-variable-stiffness-mechanism, 2023. GitHub.
[15] J. E. Shigley, *Shigley's mechanical engineering design*. Tata McGraw-Hill Education, 2011.
[16] F. Cosmi and A. Dal Maso, "A mechanical characterization of sla 3d-printed specimens for low-budget applications," *MATERIALS TODAY-PROCEEDINGS*, vol. 32, pp. 194–201, 2020.
[17] W. D. Callister, *Fundamentals of materials science and engineering : an interactive e-text / William D. Callister, Jr*. New York ;: Wiley, 2001. Includes bibliographical references and index.
[18] Formlabs, "Materials library." https://formlabs.com/uk/materials/, 2019. GitHub.